

Decoding quantum criticality from fermionic/parafermionic topological states

Zi-Qi Wang¹, Guo-Yi Zhu¹, and Guang-Ming Zhang^{1,2}

¹*State Key Laboratory of Low-Dimensional Quantum Physics and
Department of Physics, Tsinghua University, Beijing 100084, China.*

²*Collaborative Innovation Center of Quantum Matter, Beijing 100084, China.*

(Dated: April 21, 2022)

Under an appropriate symmetric bulk bipartition in a one-dimensional symmetry protected topological phase with the Affleck-Kennedy-Lieb-Tasaki matrix product state wave function for the odd integer spin chains, a bulk critical entanglement spectrum can be obtained, describing the excitation spectrum of the critical point separating the topological phase from the trivial phase with the same symmetry. Such a critical point is beyond the standard Landau-Ginzburg-Wilson paradigm for symmetry breaking phase transitions. Recently, the framework of matrix product states for topological phases with Majorana fermions/parafermions has been established. Here we first generalize these fixed-point matrix product states with the zero correlation length to the more generic ground-state wave functions with a finite correlation length for the general one-dimensional interacting Majorana fermion/parafermion systems. Then we employ the previous method to decode quantum criticality from the interacting Majorana fermion/parafermion matrix product states. The obtained quantum critical spectra are described by the conformal field theories with central charge $c \leq 1$, characterizing the quantum critical theories separating the fermionic/parafermionic topological phases from the trivial phases with the same symmetry.

I. INTRODUCTION

Since the discovery of topological phases of matter, it has been drawn more and more attention. One of the most prominent signature of topological phases of matter is the bulk-edge correspondence. For example, the topological quantum field theory describing the bulk of the fractional quantum Hall states is in one-to-one correspondence with the conformal field theory characterizing its edge excitations¹. As a manifestation of this correspondence, Li and Haldane has shown in a fractional quantum Hall system that the entanglement spectrum of the bulk describes the effective low-energy spectrum of the edge physics², which was later proved by Qi et. al. in a general quantum Hall system³. In this regards, the concept of entanglement introduced from quantum information provides a quite useful tool to characterize the topological phases in condensed matter systems.

A natural question that follows is, what more we can learn from the entanglement of the bulk of a topological phase? Is it possible to encapsulate the information of the quantum critical points adjacent to this topological phase? At first glance, this may sound crazy because there could be many paths to drive one phase to another, undergoing different quantum critical points. However, the phase transition between topological phases shares some universal features with the gapped topological phase, like the quantum Hall plateau transition in integer quantum Hall phases is uniquely determined by the topological number of the adjacent quantum Hall phases. In fact, in the integer quantum Hall systems and some other symmetry-protected topological states, the topological phase transition can be viewed as the result of quantum percolation of the topological edge modes into the bulk⁴. This implies that via the edge physics, the bulk entanglement spectrum has the potential to encode

information on the topological quantum criticality. Indeed, it is already verified in the AKLT states and integer quantum Hall systems⁵⁻⁷, demonstrating a bulk-edge-criticality correspondence.

But it remains elusive to explore the possibility of decoding topological quantum criticality from a strongly interacting system with long-range entanglement. As in the one-dimensional fermionic systems, the interacting topological phases of matter without protecting symmetry fall into the \mathbb{Z}_2 classification⁸. The only nontrivial topological phase is the Kitaev Majorana topological state with hosting an unpaired Majorana zero mode on the edges. If we go beyond the anomalous free constraint, a natural generalization of the Majorana topological state is the \mathbb{Z}_N parafermion topological state with the defining property of an unpaired parafermion zero mode on the edges. So it would be interesting to see whether such a bulk-edge-criticality correspondence is still valid in the interacting fermionic/parafermionic topological phases via the bulk entanglement spectrum. Were it be true, this would strongly support the bulk entanglement study to provide a universal recipe in one-dimensional systems to extract topological quantum criticality without fine tuning Hamiltonian.

While it is a challenging task to solve a strongly interacting parafermionic Hamiltonian even in one dimension, the bulk entanglement study has the privilege that all you need is the ground state wave-function with a finite correlation length. In general, the matrix product states (MPS) in one dimension or tensor-network states in two dimension have become a powerful ansatz to capture the essential feature of the topological ground states. In particular, the fermionic MPS of the \mathbb{Z}_2 Majorana topological phase has been established⁹, which is the minimal description of the exact ground state of the Kitaev Majorana chain. Our latest work further generalizes this

idea to construct the fixed-point MPS for the gapped \mathbb{Z}_3 parafermionic topological phase¹⁰ and the more generalized \mathbb{Z}_N parafermionic topological MPS. With these new developments, it is much more efficient to study all kinds of bulk entanglement spectra.

In this paper, we first generalize the fixed-point \mathbb{Z}_3 parafermionic MPS to a more generic topological \mathbb{Z}_N parafermionic MPS with a tunable correlation length. For the wave functions with a finite correlation length, we show that the topological edge modes are coupled with the tunable correlation strength. By introducing an extensive sublattice bipartition, we can derive the bulk entanglement Hamiltonian that describes a reduced one-dimensional system with interactions of topological edge modes. Under the symmetric bipartition with the \mathbb{Z}_2 fermionic or \mathbb{Z}_3 parafermionic topological states in particular, the bulk entanglement Hamiltonians are shown to follow the behavior of the 1+1 space-time dimensional conformal field theories, characterizing the topological quantum critical points that separate the corresponding topological phase from the trivial phase with the same symmetry. Altogether, we hope that these nontrivial calculations could evidence a tendency of generalizing the bulk-edge correspondence to the *bulk-edge-criticality* correspondence.

The rest of the paper will be organized as follows. In Sec. II, we consider the generic \mathbb{Z}_N parafermion topological MPS and discuss its correlation length. Then we study the single block bipartition for the parafermionic MPS and its entanglement spectrum which mimics the edge physics in Sec.III. In Sec. IV, we introduce the procedure of symmetric bulk bipartition to derive the corresponding reduced density matrix and the bulk entanglement Hamiltonian. Next we perform exact numerical diagonalization to the entanglement Hamiltonians and obtain the critical entanglement spectra for the \mathbb{Z}_2 Majorana and \mathbb{Z}_3 parafermionic topological phases in Sec. V. Finally the discussion of our result and a brief summary are given in Sec. VI. Some related discussions are included in the Appendices.

II. \mathbb{Z}_N PARAFERMIONIC MPS

In this section we first construct a general \mathbb{Z}_N parafermion topological MPS with a finite correlation length, which is also supported by the fractionalized Majorana/parafermion zero modes on the edges. Let's start by introducing the basics of parafermions. In a superconducting system, it is well-known that the $\mathbb{U}(1)$ charge symmetry of fermions is usually broken down to the discrete symmetry \mathbb{Z}_2 . Namely, the particle number conservation is broken down to the number parity conservation. Causality forbids to break this \mathbb{Z}_2 parity symmetry further. Therefore, the fermionic Hilbert space as a super-vector space can be decomposed into the odd and even parity sectors: $\mathbb{H} = \mathbb{H}_0 \oplus \mathbb{H}_1$. Mathematically, this \mathbb{Z}_2 super-vector space can be generalized to a \mathbb{Z}_N

super-vector space $\mathbb{H} = \mathbb{H}_0 \oplus \mathbb{H}_1 \oplus \dots \oplus \mathbb{H}_{N-1}$. Indeed, the exotic parafermions arising from the fractionalized topological insulator systems coupled to alternating ferromagnets and superconductors just live in this super-vector space. The creation or annihilation operators of \mathbb{Z}_N parafermions are the generalizations of the Majorana fermions that satisfy

$$\chi_l^N = 1, \quad \chi_l^\dagger = \chi_l^{N-1}, \quad \chi_l \chi_{l'} = e^{i\frac{2\pi}{N}} \chi_{l'} \chi_l, \quad (1)$$

for $l < l'$. It is easy to check that Majorana fermions fit into the case of $N = 2$. Unlike the bosons, the many-body states of parafermions are the \mathbb{Z}_N -graded tensor product of the single-particle states:

$$|k_1, k_2, \dots, k_N\rangle = |k_1\rangle \otimes_g |k_2\rangle \otimes_g \dots \otimes_g |k_N\rangle, \quad (2)$$

where k ranges from 0 to $N-1$. Exchanging parafermions are mathematically expressed as an isomorphism for the graded super-vectors as

$$\begin{aligned} \mathcal{F}\left(|k_l\rangle \otimes_g |j_{l'}\rangle\right) &= e^{i\frac{2\pi}{N} k_l j_{l'}} |j_{l'}\rangle \otimes_g |k_l\rangle, \\ \mathcal{F}\left(\langle k_l| \otimes_g \langle j_{l'}|\right) &= e^{-i\frac{2\pi}{N} k_l j_{l'}} \langle j_{l'}| \otimes_g \langle k_l|, \end{aligned} \quad (3)$$

where $l < l'$. An inner product can be defined by mapping the dual vector space to a complex number i.e. $\mathcal{C} : \mathbb{V}_F^* \otimes \mathbb{V}_F \rightarrow \mathbb{C}$:

$$\mathcal{C}\left(\langle k_l| \otimes_g |j_{l'}\rangle\right) = \langle k_l|j_{l'}\rangle = \delta_{k_l - j_{l'}}. \quad (4)$$

It should be noted that \mathcal{C} and \mathcal{F} commute, which will be repeatedly used in this paper. Moreover, the way which the parafermion operator acts on the many-body parafermion state follows as

$$\begin{aligned} \chi_{2j} |\dots k_j \dots\rangle &= e^{i\frac{2\pi}{N} (\sum_{i \leq j} k_i - \frac{N+1}{2})} |\dots (k_j - 1)_{\text{mod } N} \dots\rangle, \\ \chi_{2j-1} |\dots k_j \dots\rangle &= e^{i\frac{2\pi}{N} \sum_{i < j} k_i} |\dots (k_j - 1)_{\text{mod } N} \dots\rangle, \end{aligned} \quad (5)$$

where the phase string arises from the non-local commutation relation of parafermions. Any parafermionic state should belong to the special super-vector space with a definite charge detected by the charge operator:

$$\hat{Q} = \prod_{l=1}^L (-e^{i\frac{\pi}{N}} \chi_{2l-1}^\dagger \chi_{2l}), \quad \hat{Q}|\Psi_m\rangle = e^{i\frac{2\pi}{N} m} |\Psi_m\rangle, \quad (6)$$

where $|\Psi_m\rangle$ is a many-body state defined in the \mathbb{H}_m with the charge $m = 0, 1, 2, \dots, N-1$. Recently, the MPS for the one-dimensional parafermionic topological phase has been constructed^{10,11}. It can be expressed in terms of a series of local parafermionic graded tensor:

$$|\Psi_m\rangle = \mathcal{C}\left(\hat{\tau}^{-m} \hat{\mathbf{A}}_1 \otimes_g \dots \otimes_g \hat{\mathbf{A}}_L\right). \quad (7)$$

Each local site is associated with a graded product of super-vectors:

$$\hat{\mathbf{A}} \equiv \sum_{\alpha\beta k} A_{\alpha\beta}^{[k]} |\alpha\rangle \otimes_g |k\rangle \otimes_g |\beta\rangle, \quad (8)$$

where $|k\rangle$ denotes the Fock parafermion mode and $|\alpha\rangle$ and $|\beta\rangle$ are two virtual parafermion modes living in super-vector space \mathbb{V}_F and dual-super-vector space \mathbb{V}_F^* , respectively. Contraction of the virtual modes ties the neighboring sites by maximally entangling bonds, leading to a compact form as

$$|\Psi_m\rangle = \sum_{k_1, \dots, k_L} \text{ctr} \left(\tau^{-m} A^{[k_1]} \dots A^{[k_L]} \right) |k_1 \dots k_L\rangle, \quad (9)$$

with the total charge $m = \sum_l k_l \bmod N$. Here τ is the generator of the \mathbb{Z}_N group with its matrix element $\tau_{\alpha, \beta} = \delta_{(\beta - \alpha - 1) \bmod N}$. For the closed boundary system, there is a one-to-one correspondence between the total charge and the boundary conditions. Specifically, in the \mathbb{Z}_2 Majorana case, $m = 0$ corresponds to the even parity state under the anti-periodic boundary condition, while $m = 1$ to the odd parity state under the periodic boundary condition. A graphic representation for the local tensor is given in Appendix A. Motivated by an exact ground state in the interacting fermionic system¹², we generalize the parafermionic MPS to a generic \mathbb{Z}_N parafermionic MPS with a tunable correlation length, and the local tensor is expressed as

$$A_{\alpha, \beta}^{[k]} = C e^{-k\phi/N} \delta_{(\beta - \alpha - k) \bmod N}, \quad (10)$$

where ϕ is a tuning parameter playing the similar role to the chemical potential for the local charge k ranging from 0 to $N - 1$, and C is the normalization factor. As shown later, the correlation length can be continuously tuned by ϕ . What's amazing is that despite the arbitrary long correlation length tuned by ϕ , this MPS always maintains to be topologically nontrivial and characterizes the topological phase of \mathbb{Z}_N parafermions away from fixed point. Essentially this is due to the gauge symmetry

$$\tau^\dagger A^{[k]} \tau = A^{[k]}. \quad (11)$$

More evidences can be found in the later section. We have to mention that Eq. (10) does not exhaust all possibilities of the MPS with $N > 2$, which maintains the gauge symmetry and topological nontrivial. In fact for the generic \mathbb{Z}_N case, there can be at most $N - 1$ independent parameters controlling the relative distribution of the N physical channels on each site $A_{\alpha, \beta}^{[k]} \rightarrow a_k \delta_{(\beta - \alpha - k) \bmod N}$ without breaking the gauge symmetry. Here and after, we'll abbreviate the modulo N in the arguments of all delta function for convenience. It should be mentioned that the case of \mathbb{Z}_3 is essentially equivalent to the MPS proposed by Fernando, et. al.¹³. The charge basis we adopt is nevertheless a better and more natural. Despite its similarity with the bosonic MPS, the Majorana/parafermionic MPS is dramatically distinct in the following two aspects: the matrix structure is subjected to the constraint by the intrinsic \mathbb{Z}_N symmetry, and the nontrivial commutation relation of the (para)fermions brings in a nontrivial phase factor when performing a contraction or permutation.

Now let's come to discuss the correlation of the general MPS wave function. A generic two-body correlator $\langle \psi | \hat{O}_i \hat{O}_j | \psi \rangle$ can be cast into the tensor network, which involves a consecutive mapping through the transfer matrix defined as:

$$\mathbb{E}_{(\alpha\alpha'), (\beta\beta')} = \sum_k A_{\alpha, \beta}^{[k]} \bar{A}_{\alpha', \beta'}^{[k]}. \quad (12)$$

Note that unlike the bosonic case, the correlator could involve additional phase factor counting the total charge between the lattice sites i and j due to the parafermion commutation. Nevertheless, this seemingly non-local phase can be attributed to a local charge detector deposited on the virtual bonds at the sites i and j only, see Appendix A for detail. According to a quite standard MPS scheme, the spectrum of this transfer matrix determines the correlation length of the wave function. To diagonalize this transfer matrix, we can recast the eigen-equation of the transfer matrix into a complete positive map:

$$\begin{aligned} \sum_k A^{[k]} R_{n,j} \left(A^{[k]} \right)^\dagger &= \lambda_n R_{n,j}, \\ \sum_k \left(A^{[k]} \right)^\dagger L_{n,j} A^{[k]} &= \lambda_n L_{n,j}, \end{aligned} \quad (13)$$

in which the right eigen-vector is reshaped into the matrix $R_{n,j}$, the left eigen-vector is reshaped into the matrix $L_{n,j}$, n labels different eigenvalues, and j labels eigen-vectors with the degenerate eigen-value. The eigen-equation can be immediately solved as

$$\begin{aligned} (R_{n,j})_{\alpha, \alpha'} &= \frac{1}{\sqrt{N}} e^{-i2\pi n \alpha / N} \delta_{\alpha - \alpha' - j}, \\ (L_{n,j})_{\beta', \beta} &= \frac{1}{\sqrt{N}} e^{i2\pi n \beta / N} \delta_{\beta - \beta' - j}, \end{aligned} \quad (14)$$

with the eigenvalues $\lambda_n = |\lambda_n| e^{i\theta_n}$, where

$$\begin{cases} |\lambda_n| = \left[1 + \left(\frac{\sin \frac{\pi n}{N}}{\sinh \frac{\phi}{N}} \right)^2 \right]^{-\frac{1}{2}}, \\ \theta_n = \tan^{-1} \frac{\sin \left(\frac{2\pi n}{N} \right)}{\cos \left(\frac{2\pi n}{N} \right) - e^{2\phi/N}}. \end{cases} \quad (15)$$

The global factor C in Eq. (10) is chosen to make the largest eigenvalue $\lambda_0 = 1$, ensuring the normalization condition of the MPS in the thermodynamic limit. It is found that the transfer spectrum is N -fold degenerate so that both n and j ranges from 0 to $N - 1$. The degeneracy is no surprise because the transfer matrix inherits the gauge symmetry from the local matrix as a signature of the topological nontriviality: $(1 \otimes \tau^\dagger) \mathbb{E} (1 \otimes \tau) = \mathbb{E}$. The eigenvectors within the degenerate subspace are therefore related by $(1 \otimes \tau)$ or $(\tau \otimes 1)$. And yet $N - 1$ among them, i.e. those non-diagonal ones with $j \neq 0$ are redundant and do not contribute to the physical consequences. The origin of redundancy is due to the mismatch between the virtual bond dimension N and the

parafermion quantum dimension \sqrt{N} . The physically relevant ones are the diagonal ones $R_{n,0}$ and $L_{n,0}$. Since $|\lambda_n| \leq 1$ and $\lambda_n = \bar{\lambda}_{N-n}$, the sub-dominant eigenvalue $\lambda_1 = \bar{\lambda}_{N-1}$ contributes to the correlation in the thermodynamic limit:

$$\langle \psi | \hat{O}_i \hat{O}_j | \psi \rangle - \langle \psi | \hat{O}_i | \psi \rangle \langle \psi | \hat{O}_j | \psi \rangle \propto \text{Re} \lambda_1^{|j-i|}, \quad (16)$$

and the more detail is given in Appendix B. Therefore the correlation length ξ can be defined by:

$$\xi^{-1} = \frac{1}{2} \ln \left[1 + \left(\frac{\sin \frac{\pi}{N}}{\sinh \frac{\phi}{N}} \right)^2 \right]. \quad (17)$$

Note that the correlation length is always finite except when $\phi = 0$, concurring with the fixed-point MPS discussed before¹⁰. By varying the parameter ϕ , we can continuously tune the correlation length of the topological parafermionic MPS.

III. ENTANGLEMENT SPECTRUM AND EDGE PHYSICS

With the topological wave function, we can perform various bipartitions and study the corresponding entanglement spectrum to probe the topological nontriviality therein. Besides the gauge symmetry, the topological nontriviality manifests much more explicitly on the existence of fractionalized edge modes. To reach the boundary theory, we can make use of the bulk-edge correspondence, i.e., studying the single block entanglement spectrum^{2,3}.

More specifically, we can bipartite the bulk into one block of l sites and its complement part, as shown in Fig. 1(a). By tracing out the complement part, we're left with a reduced density matrix ρ_r describing the block. Since the bulk is gapped, the low energy physics of the block is reflected on its gapless edge excitations. There is an isometry transformation V that maps the block physical parafermions χ to the effective edge parafermions ψ , preserving the spectrum of the eigenvalues: $\text{spec}(\rho_r) = \text{spec}(V^\dagger \rho_r V)$. In the following we mainly deal with the effective reduced density matrix $\tilde{\rho}_r \equiv V^\dagger \rho_r V$, which is supported on the effective edge degrees of freedom and faithfully characterizes the low-energy physics of the block. In fact, by treating the complement part as the environment, we can rewrite the reduced density matrix in terms of the thermal density matrix as

$$\tilde{\rho}_r \equiv e^{-\tilde{H}_{\text{ent}}}, \quad (18)$$

which defines the entanglement Hamiltonian as the negative logarithm of the reduced density matrix. The entanglement Hamiltonian was conjectured and further proved to faithfully characterize the low-energy sectors of the boundary theory in the quantum Hall systems^{2,3}. In the following we explain how to extract the entanglement Hamiltonian using the MPS.

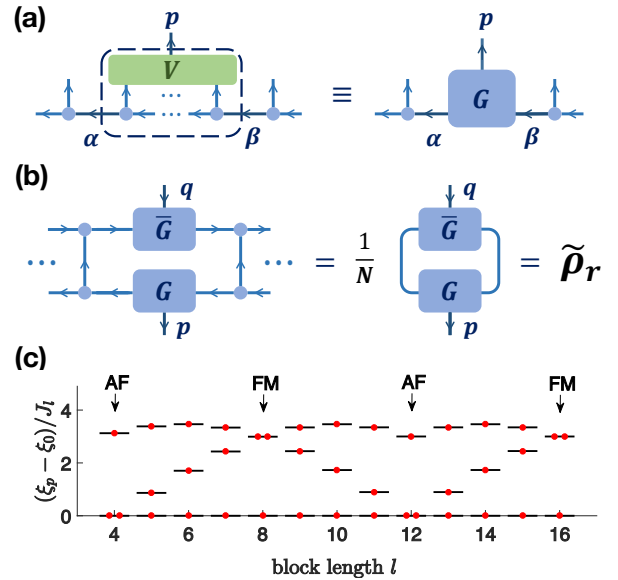


FIG. 1: (a) Applying an isometry to the block of l sites leads to the coarse grained MPS. An arrow pointing outwards from one site is associated to a super-vector space \mathbb{V}_F while inwards to \mathbb{V}_F^* . (b) The reduced density operator of a single block. (c) The block entanglement spectrum of \mathbb{Z}_3 case. The spectra structure experiences a periodicity with respect to the block length. Two typical phases are remarked as the ferromagnetic (FM) and anti-ferromagnetic (AFM) between two edge modes. Here we choose $\phi \simeq 1.5076$.

First we coarse grain the MPS by blocking the local matrices of l -sites altogether and treating it as a matrix $\tilde{A}_{\alpha\beta}^{\{k_i\}}$ that linearly maps the left- and right- virtual degrees of freedom ($\alpha\beta$) into the physical degrees of freedom $\{k_i\}$. To extract the relevant features, we perform a singular value decomposition to the matrix: $\tilde{A} = USV^\dagger$, where V is exactly the isometry transformation, S is a diagonal matrix with singular values that characterize the distributive weights of relevant degrees of freedom, and U as the isometry that assembles the virtual modes to be the effective degrees of freedom. According to the relations $\tilde{A}\tilde{A}^\dagger = US^2U^\dagger$ and

$$(\tilde{A}\tilde{A}^\dagger)_{(\alpha\beta),(\alpha'\beta')} = \sum_{n,j} (R_{n,j})_{\alpha,\alpha'} \lambda_n^l (L_{n,j})_{\beta',\beta}. \quad (19)$$

we can deduce U and S by diagonalizing $\tilde{A}\tilde{A}^\dagger$. Therefore U is found with its matrix elements as $U_{(\alpha,\beta),p} = \delta_{\beta-\alpha-p}/\sqrt{N}$ and the nonzero singular values in S are given by

$$s_p = \sqrt{\sum_{n=0}^{N-1} \lambda_n^l e^{i\frac{2\pi}{N}np}}, \quad (20)$$

where p ranges from 0 to $N-1$ and the quantity inside the square root keeps positively definite. The Eq.(20) shows how the singular values rely on the eigenvalue of the transfer matrix and the block length l explicitly. It

is worth noticing that, although the two edges together ($\alpha\beta$) appear to have N^2 degrees of freedom, only N among them are relevant. This is a signature of the fractionalization, rooted in the quantum dimension of edge mode being \sqrt{N} . Finally we can project \tilde{A} onto the relevant degrees of freedom living on edges by the isometry $G \equiv \tilde{A}V = US$ with its matrix elements

$$G_{\alpha,\beta}^{[p]} = \frac{s_p}{\sqrt{N}} \delta_{\beta-\alpha-p}. \quad (21)$$

When the length of the complement of the block is sufficiently long, shown in Fig. 1(b), it is straightforward to obtain $\tilde{\rho}_r$ independent of the boundary condition:

$$(\tilde{\rho}_r)_{p,q} = \text{tr} \left[G^{[p]} R_{0,0} \left(G^{[q]} \right)^\dagger L_{0,0} \right] = \frac{1}{N} s_p^2 \delta_{p-q}, \quad (22)$$

where $L_{0,0}$ and $R_{0,0}$ are the matrices reshaped from the eigenvectors of the transfer matrix corresponding to the maximum eigenvalue. It is obvious that $\tilde{\rho}_r$ is already in a diagonal form with eigenvalues s_p^2/N . The entanglement spectrum as the eigenvalues of \hat{H}_{ent} is thus given by

$$\xi_p = -\ln \left(\frac{1}{N} \sum_{n=0}^{N-1} \lambda_n^l e^{\frac{i2\pi}{N} np} \right). \quad (23)$$

From the expression, we find that the complete spectrum decays exponentially with the block length l : $\xi_p - \xi_0 \propto e^{-l/\xi} \equiv J_l$.

To give a concrete example, we consider the \mathbb{Z}_2 Majorana topological state as a parent state. There are only two levels in the block entanglement spectrum labeled by even and odd parity respectively, and the gap between them is proportional to J_l . To understand the spectrum more transparently, we need the entanglement Hamiltonian that indicates how the edge degrees of freedom interact with each other. Taking the logarithm of $\tilde{\rho}_r$ and expressing it back in terms of operators, we can obtain the entanglement Hamiltonian to the leading order of J_l :

$$\hat{H}_{\text{ent}} \simeq iJ_l \gamma_1 \gamma_2 + \ln 2 + \mathcal{O}(J_l^2), \quad (24)$$

which describes the coupling between the two edge Majorana zero modes through the bulk. The coupling strength is exponentially suppressed with correlation length as the characteristic length. When $l/\xi \gg 1$, the two edge Majorana zero modes tend to be decoupled, and the excited level tends to collapse to the ground state level. We then go to a more nontrivial concrete demonstration with \mathbb{Z}_3 parafermion topological state. Similarly, the spectra is exposed to a global exponential suppression due to the dependence of J_l on l . But we are more interested in the relative structure of the entanglement spectrum. The rescaled spectrum for the \mathbb{Z}_3 case is shown in Fig. 1(c). It is visualized that the relative structure shows certain periodicity.

Actually, for the generic \mathbb{Z}_N cases with $N \geq 3$, there is an asymptotic periodicity of $2\pi/N$ to the leading order of J_l :

$$\xi_p \simeq \ln N - 2J_l \cos \left(\frac{2\pi p}{N} + l\theta_1 \right) + \mathcal{O}(J_l^2). \quad (25)$$

To understand the spectrum more transparently, the entanglement Hamiltonian is derived as:

$$\hat{H}_{\text{ent}} \simeq \left[e^{i(\frac{\pi}{N} + l\theta_1)} J_l \psi_1^\dagger \psi_2 + h.c. \right] + \ln N + \mathcal{O}(J_l^2), \quad (26)$$

which describes the leading coupling between the two effective parafermionic modes ψ_1 and ψ_2 of the edges respectively. Due to the exponentially decaying of coupling strength, the leading term is sufficient to characterize the spectrum when block length l is large enough. Now it is quite clear that the periodicity of the level structure arises from the coupling phase cycling with the block length. The cases with $l\theta_1 = (2k+1)\pi$ and $l\theta_1 = 2k\pi$ are of particular importance. The former corresponds to the ferromagnetic (FM) coupling of two edge modes in \mathbb{Z}_3 case^{14,15}, exhibiting non-degenerate lowest level and two-fold degenerate excited level, while the latter corresponds to the anti-ferromagnetic (AFM) coupling of two edge modes, displaying two-fold degenerate lowest level and non-degenerate excited level. In the next section we'll show that, depending on the coupling phase, the distinct interactions lead to distinct quantum critical theories.

IV. SYMMETRIC BULK BIPARTITION AND ENTANGLEMENT HAMILTONIAN

While the entanglement Hamiltonian derived from the single block bipartition is shown to describe the edge physics, it is absolutely incapable of describing the bulk because it is one-dimension lower than the bulk. In this section we introduce an extensive sublattice bipartition that yields an entanglement Hamiltonian describing the bulk physics.

The basic idea of decoding topological quantum criticality from a gapped topological phase⁵ lies in having the fractionalized edge degrees of freedom to couple with each other and percolate into the reduced bulk subsystem. This can be manufactured by a sublattice bipartition of the bulk into L_A pairs of alternating interlaced A and B sub-blocks, and tracing out the sub-system B and leaving A as a system of interest. Since the bulk is gapped, the low-energy physics of subsystem A is dominated by the extensive fractionalized edge degrees of freedom, as shown in Fig. 3(a). Distinct from the former single block bipartition that yields (0+1) dimensional entanglement Hamiltonian describing the edge physics, this extensive interlaced bipartition gives rise to a (1+1) dimensional entanglement Hamiltonian characterizing the bulk properties.

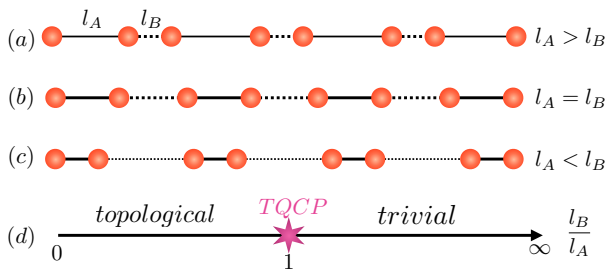


FIG. 2: (a), (b), (c) The three topologically distinct phases driven by distinct relative block length are shown schematically. The red dots remark the fractionalized edge particles as the low energy effective degrees of freedom of each block in the sub-system A. Solid line corresponds to the sub-system A while the dashed line stands for the sub-system B that is to be traced out. The coupling strength between edge particles decay exponentially with the block length so the relative strong coupling is highlighted with bold line. (d) A schematic phase diagram. The topological quantum critical point is guaranteed to be self-dual and translational invariant.

Depending on the relative block length of l_A and l_B , the subsystem A itself can fall in either topological or trivial phase, as shown in Fig. 2. This can be visualized in two limits: when l_B is relatively small, the subsystem A is essentially the same phase with the original gapped topological phase; when l_A is small enough, it falls into a product state of dimers. As one cannot start from the topological phase and enter into the trivial phase without experiencing a quantum critical point, it is expected that the subsystem A could be critical when l_A and l_B are comparable. Especially, in \mathbb{Z}_2 Majorana case, the topological phase is related to the trivial phase by a duality transformation which can be implemented by the single site translation of the Majorana modes¹⁶. As a result, the quantum critical point separating the \mathbb{Z}_2 Majorana topological phase from the trivial phase is translational invariant with respect to Majorana lattice¹⁷. This implies that the topological critical point is robustly pinned at $l_A = l_B$ despite the presence of even higher order interactions. This scenario could possibly be generalized to the \mathbb{Z}_N case, i.e. $l_A = l_B \equiv l$ to ensure that the coupling strength between the fractionalized edge modes is translational invariant. We call this symmetric bulk bipartition.

We first group every l sites together and apply the isometry transformation V to obtain a coarse grained chain with block tensor G . By tracing out the alternating B blocks, a parafermionic density operator in the form of a tensor-network is shown in Fig. 3. However, the scheme of tracing B is far less straightforward, because it needs permuting the physical parafermions which would inevitably result in a highly non-local phase. Nevertheless, this problem can be circumvented by a trick making use of the tensor-network formalism as a quantum circuit. Namely, the non-local phase factor arising from commuting parafermions can be shuffled and redistributed into each site locally at the cost of an additional bond that

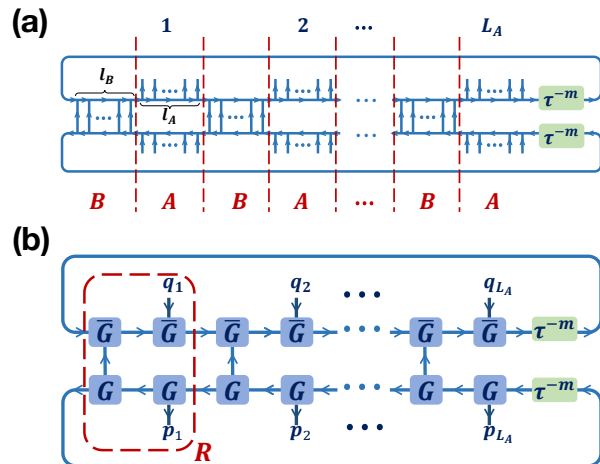


FIG. 3: (a) A graphical tensor-network representation of the reduced density operator after a symmetric bulk bipartition. Here both of bra and ket charge m topological chains are divided into alternating L_A pairs of interlaced A and B parts with respective length l_A, l_B . (b) By coarsened graining both chains, the simplified repeating element is denoted as R , and the arrows indicate that this tensor-network still carries parafermionic operators and is not available for the direct numerical calculation. When all parafermionic states in the part B are contracted, the reduced density operator becomes a conventional tensor-network, at the prize of additional bonds playing the similar role of the Jordan-Wigner phase string.

tracks and records the total charge of all the parafermions to the left of certain site. In this way, the parafermionic density operator turns into a more conventional tensor-network that is amenable to direct numerical calculation (see more detail in Appendix C). Moreover, as the parafermion has fractional quantum dimension \sqrt{N} , the bond dimension of the tensor network can be effectively reduced from N^2 to N . Thus the repeating element of the matrix product operator (MPO) is derived to be a six-rank tensor

$$R_{(\alpha l), (\beta r)}^{[p, q]} = \frac{1}{N^2} e^{i2\pi(\beta - \alpha - p) \frac{l}{N}} \delta_{r-l-p+q} s_p s_q s_{(\beta - \alpha - p) \bmod N}^2 \quad (27)$$

where p denotes the effective degrees of freedom for each block, α, β are the remained virtual bonds that are to be contracted, and l (r) inputs (outputs) the accumulated charge to the left of the site, the four singular values come from the four blocks respectively, and the phase factor accounts for the commutation between physical parafermions before their contraction. It is worth noticing that the additional bonds essentially play the similar role as the Jordan-Wigner phase string, which is inevitable when one tries to turn something fermionic into bosonic.

While the reduced density operator in the form of MPO is already available for direct numerical calculation, we're here to give an analytical derivation of the final expression of the reduced density operator. In essence we're going to grain L_A number of R tensor together and con-

tract all the internal bonds, leaving only the physical ones and the boundary bonds. We denote this intermediate block tensor as $\tilde{R}_{\alpha,\beta r}^{\{p,q\}}(L_A)$, which depends on the length of subsystem L_A and carries both physical and boundary bonds. Finally contracting the boundary bonds in this block tensor yields the reduced density matrix, as shown in Fig. 3(b). By noticing that the intermediate block tensor has a recursion relation:

$$\tilde{R}_{\alpha,\beta r}^{\{p,q\}}(L_A) = \sum_{\beta',r'} \tilde{R}_{\alpha,\beta'r'}^{\{p,q\}}(L_A - 1) R_{\beta'r',\beta r}^{[p_{L_A}, q_{L_A}]}, \quad (28)$$

we can derive the explicit form of the intermediate block tensor, and then contract the boundary bonds to derive the reduced density operator as the form

$$\hat{\rho}_A = C' \left(\prod_{j=1}^{L_A} \hat{S}_j \right) \left(\prod_{j=1}^{L_A} \hat{I}_j \right) \left(\prod_{j=1}^{L_A} \hat{S}_j \right), \quad (29)$$

where C' is the normalization factor and \hat{S} is an operator form of the diagonal singular matrix for one block. Physically \hat{S} stands for the coupling between the edge fractionalized particles of one block, while \hat{I} describes the hopping between fractionalized edge particles from the adjacent blocks:

$$\begin{aligned} \hat{S}_j &= \sqrt{\sum_{k=0}^{N-1} \lambda_k^l \left(-e^{\frac{i\pi}{N}} \psi_{2j-1}^\dagger \psi_{2j} \right)^k}, \\ \hat{I}_j &= \sum_{k=0}^{N-1} \lambda_k^l \left(-e^{\frac{i\pi}{N}} \psi_{2j}^\dagger \psi_{2j+1} \right)^k. \end{aligned} \quad (30)$$

With the reduced density operator, the bulk entanglement Hamiltonian is thus obtained

$$\hat{H}_A \equiv -\ln \hat{\rho}_A, \quad (31)$$

which is in general a complicated Hamiltonian with long-range interactions but can be controlled by the correlation length of the parent gapped wave function.

In the following section we'll numerically perform exact diagonalization for the reduced density matrix in the form of the MPO, and demonstrate that the exact numerical results are consistent with the analytical form of the entanglement Hamiltonian up to the leading orders.

V. EXACT NUMERICAL RESULTS OF CRITICAL ENTANGLEMENT SPECTRA

The main focus of this section is on the bulk entanglement Hamiltonian Eq.(31) defined for the symmetric bulk bipartition. We'll perform exact diagonalization and obtain a critical spectrum for the entanglement Hamiltonian labeled by the charge and momentum good quantum numbers. In the following, we'll first introduce the momentum and charge quantum numbers, and then show

the numerical data for two concrete examples of \mathbb{Z}_2 Majorana phase and \mathbb{Z}_3 parafermion phase, respectively. Both of them exhibit quantum critical behavior characterized by conformal field theories.

A. Symmetries of the entanglement Hamiltonian

Before doing numerical calculation, we look at the symmetries of the entanglement Hamiltonian. In fact, the symmetries are inherited from the parent topological state. The topological states with different charges correspond to different boundary conditions. As we mentioned early, the \mathbb{Z}_N charge symmetry \hat{Q} is intrinsic and cannot be broken. So we always have charge as a good quantum number.

Next we consider the translation symmetry and boundary conditions. As the symmetry of the entanglement Hamiltonian follow from the parent topological state, we look into the symmetry actions in the parent state. Since $\text{tr}(\tau^{-m} A^{[k_1]} \dots A^{[k_L]}) = \text{tr}(\tau^{-m} A^{[k_L]} A^{[k_1]} \dots A^{[k_{L-1}]})$ due to the gauge symmetry, there exists a modified 'bi-translation' symmetry for the \mathbb{Z}_N topological state with charge- m . The bi-translation acts on the parafermions in the following way:

$$\begin{cases} \tilde{T} \chi_j \tilde{T}^\dagger &= e^{-i\frac{2\pi}{N}} (\chi_2^\dagger \chi_1)^2 \chi_{j+2}, \quad \text{for } j < 2L - 1, \\ \tilde{T} \chi_{2L-1} \tilde{T}^\dagger &= e^{i(m-2)\frac{2\pi}{N}} (\chi_2^\dagger \chi_1)^2 \chi_1, \\ \tilde{T} \chi_{2L} \tilde{T}^\dagger &= e^{i(m-2)\frac{2\pi}{N}} (\chi_2^\dagger \chi_1)^2 \chi_2. \end{cases} \quad (32)$$

Such a bi-translation symmetry physically translates the parafermion lattice by two sites up to a phase factor depending on the total charge of the state, and the additional charge zero part $(\chi_2^\dagger \chi_1)^2$ plays the role of preserving the parafermion commutation relation. When $N = 2$ for the Kitaev Majorana case, $(\chi_2^\dagger \chi_1)^2 = -1$, the translation restores a familiar single site translation, corresponding to the periodic boundary condition for the odd parity parent state $m = 1$, and the anti-periodic boundary condition for the even parity parent state $m = 0$. It is more natural to see that under the modified translation the physical basis of the generic \mathbb{Z}_N parafermion wave-function changes in the following way:

$$\tilde{T} |k_1, \dots, k_{L-1}, k_L\rangle = |k_L, k_1, \dots, k_{L-1}\rangle. \quad (33)$$

So the bi-translation symmetry also gives rise to a good quantum number similar to the usual momentum. The fact that the translation by L times restores the same operator up to a charge operator is due to the non-trivial parafermion commutation relation $\tilde{T}^L \chi_j \tilde{T}^{\dagger L} = e^{i(m-1)\frac{2\pi}{N}} \hat{Q}^2 \chi_j$, leading to the consequence of shifting the momentum by a fractional value. The boundary condition of the entanglement Hamiltonian is in one-to-one correspondence with the charge of the parent topological state. We thus have

$$\tilde{T} \left(\psi_j^\dagger \psi_{j+\delta} \right)^k \tilde{T}^\dagger = \left(\psi_{j+2}^\dagger \psi_{j+2+\delta} \right)^k, \quad (34)$$

where δ denotes the neighboring lattice sites and k is a integer power. The relation $\psi_{2L_A+j} \equiv e^{i(m-1)\frac{2\pi}{N}}\psi_j$ manifests the boundary condition depending on the charge m of the parent topological state. Since \hat{H}_A is an equal weight summation of the product of these terms, it can be proved that it is invariant under the modified "bi-translation" symmetry. Moreover, the charge operator for those edge modes should be modified as

$$\tilde{Q} = e^{i\frac{2\pi}{N}m} \prod_{j=1}^{L_A} (-e^{i\frac{\pi}{N}}\psi_{2j-1}^\dagger\psi_{2j}), \quad (35)$$

where the first factor comes from the charge of the parent topological state. \tilde{Q} introduces additional charge quantum number m' for a given m , and such a modified charge operator commutes with the entanglement Hamiltonian and the modified translation,

$$[\tilde{Q}, \hat{H}_A] = [\tilde{Q}, \tilde{T}] = 0. \quad (36)$$

As a result, we can label the entanglement spectra with the momentum and charge quantum numbers simultaneously. Last but not least, we mention that the bi-translation symmetry imposed on the grouped blocks does not depend on the relative block length. While the momentum is attributed to the bi-translation symmetry, the single site translation depending on the relative block length is a much more subtle symmetry.

B. \mathbb{Z}_2 Majorana fermion criticality

As a simple example, we first consider the most familiar \mathbb{Z}_2 Majorana system. The entanglement spectrum under the symmetric bulk bipartition is shown in Fig. 4, where we choose $\phi = 2$, $l = 5$ and the largest value of $L_A = 18$. In Fig. 4(a), we show that the first two energy levels in the finite-size system linearly collapse to the ground state energy. Meanwhile we can pick out the ground state of the entanglement Hamiltonian effectively composed of L_A sites and perform the usual block bipartition to calculate the entanglement entropy. The result is shown in Fig. 4(b), where $x < L_A$ denotes the block length. The scaling of entanglement entropy follows the Calabrese-Cardy formula in the closed boundary¹⁸:

$$S(x, L_A) = \frac{c}{3} \ln \left[\frac{L_A}{\pi} \sin \left(\frac{\pi x}{L_A} \right) \right] + S_0. \quad (37)$$

The slope yields the central charge $c \simeq \frac{1}{2}$, which uniquely characterizes the free Majorana fermion CFT. Indeed, it is known that this theory describes the self-dual critical point separating the \mathbb{Z}_2 topological phase from trivial phase in Kitaev Majorana chain^{16,19,20}.

Moreover, it can be further verified that the low-energy part of the energy-momentum spectrum exactly follows the scaling law of the Ising conformal field theory. The

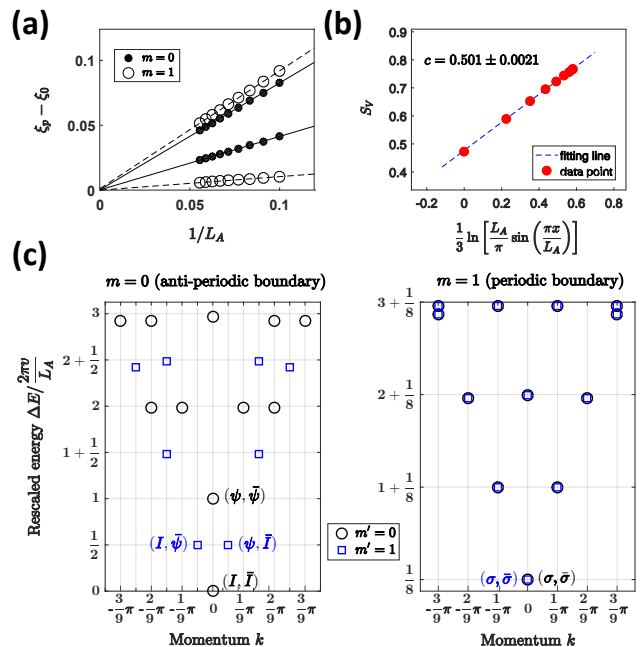


FIG. 4: (a) The finite-size scaling of the lowest two excited entanglement levels indicate a critical entanglement spectrum in the thermodynamic limit. (b) The nested entanglement entropy S_V is calculated, and the central charge is extracted as $c = 0.502 \pm 0.0021$. (c) The left entanglement spectrum is obtained from the parent topological state under the anti-periodic boundary condition ($m = 0$), while the right spectrum is calculated from the parent topological state with the periodic boundary condition ($m = 1$). m' denotes the total parity of the entanglement levels.

energy levels of the lowest primary fields with their descendants are displayed in Fig. 4(c), where the levels are shifted by a constant to set the energy of identity primary field as zero and the values of the levels are rescaled. For the even parity parent topological state ($m = 0$), the boundary condition corresponds to the anti-periodic in the Majorana fermion representation, and the Hilbert space of the subsystem A is restricted within the Neveu-Schwarz sector, which explains why the momentum could be shifted by half-integers in the left spectrum in Fig. 4(c). The corresponding energy levels are labeled by the primary fields (I, \bar{I}) , (ψ, \bar{I}) , $(I, \bar{\psi})$, $(\psi, \bar{\psi})$, where the corresponding conformal weights are $h_I = 0$ and $h_\psi = 1/2$. On the other hand, for the odd parity parent topological state ($m = 1$), the boundary condition becomes periodic, and the Hilbert space of subsystem A lies in the Ramond sector. As shown in right spectrum of Fig. 4(c), the energy levels are marked by the primary fields $(\sigma, \bar{\sigma})$ with the conformal weight $h_\sigma = 1/16$.

C. \mathbb{Z}_3 parafermion criticality with FM coupling

The \mathbb{Z}_3 parafermion system is more nontrivial because the existence of parafermions is necessarily a strongly in-

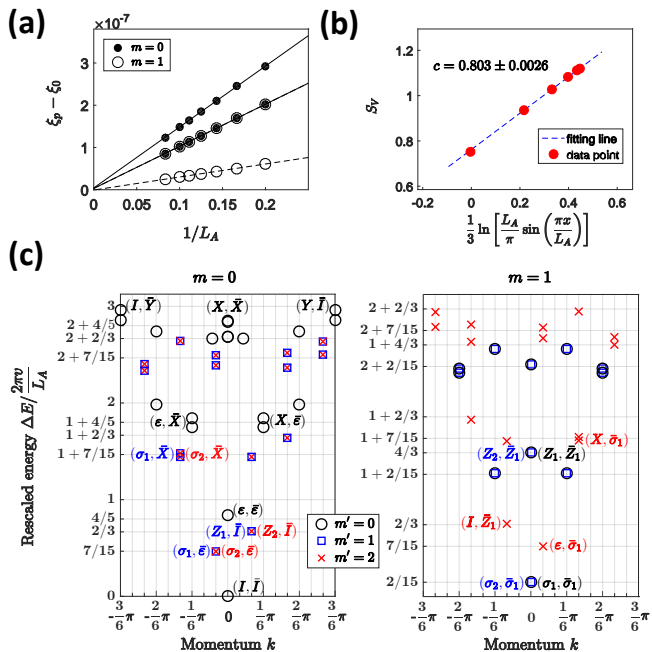


FIG. 5: (a) The finite-size scaling of the lowest two excited levels under two different boundary conditions indicate a critical entanglement spectrum in the thermodynamic limit. (b) The entanglement entropy S_V of the ground state of the entanglement Hamiltonian is calculated and the central charge is extracted as $c = 0.803 \pm 0.0026$. (c) The left spectrum is calculated from the parent topological state with $m = 0$, while the right spectrum is from the parent topological state with $m = 1$. m' denotes the total charge of the entanglement levels, and the subscript of the primary fields indicate these total charges.

interacting system. In contrast to the \mathbb{Z}_2 situation, there could be more than one quantum critical theories, depending on the phase factor of the coupling constant between every two neighboring edge parafermions. This phase factor can be tuned by the block length l in our decoding procedure. Among them two phases are prototypical: $\theta_1 = 2k\pi$ for the FM coupling and $\theta_1 = 2(k+1)\pi$ for the AFM coupling.

We first consider the FM coupling case. In the numerical calculation, the parameter is chosen as $l = 24$, $\phi \simeq 1.5076$ and the largest values of $L_A = 12$. We shall see that the energy levels of the entanglement Hamiltonian also linearly collapse to the ground state energy, as shown in Fig. 5(a). The entanglement entropy of the ground state of the entanglement Hamiltonian is also calculated and shown in Fig. 5(b), which fits into the Calabrese-Cardy formula with a central charge $c \simeq \frac{4}{5}$, confirming the \mathbb{Z}_3 parafermion CFT. Indeed, this theory describes the topological quantum phase transition from \mathbb{Z}_3 nontrivial topological phase to the trivial phase.

Furthermore, it can also be shown that the low-energy part of the spectra exactly follow the scaling law dictated by \mathbb{Z}_3 parafermion CFT, displayed in Fig. 5(c). Note that the $m = 2$ case is related to $m = 1$ by

the charge conjugate symmetry and has the same spectrum. Therefore, we only show the numerical result of $m = 0$ and $m = 1$. The energy levels for $m = 0$ can be expressed as the conformal primary fields: $(I, \bar{I}), (I, \bar{Y}), (Y, \bar{I}), (Y, \bar{Y}), (\epsilon, \bar{\epsilon}), (\epsilon, \bar{X}), (X, \bar{\epsilon}), (X, \bar{X}), (\epsilon, \bar{\sigma}), (X, \bar{\sigma}), (I, \bar{Z})$ and (Y, \bar{Z}) . The six corresponding conformal weights are $h_I = 0$, $h_\sigma = 1/15$, $h_\epsilon = 2/5$, $h_Z = 2/3$, $h_X = 7/5$, and $h_Y = 3$, respectively. Meanwhile the energy levels for $m = 1$ correspond to the conformal primary fields: $(\sigma, \bar{\sigma}), (Z, \bar{Z}), (\epsilon, \bar{\sigma}), (X, \bar{\sigma}), (I, \bar{Z})$ and (Y, \bar{Z}) . The subscripts of the primary fields represent the total parafermion charge.

D. \mathbb{Z}_3 parafermion criticality with AFM coupling

Let us now consider the AFM coupling case and perform the similar numerical calculations for $\phi \simeq 1.5076$, $l = 12$ and the largest value of $L_A = 12$. Similar to the FM case, the lowest excitation levels are scaled linearly as a function of $1/L_A$, indicating a gapless spectrum as shown in Fig. 6(a). The calculation of the ground state entanglement entropy for the entanglement Hamiltonian shown in Fig. 6(b) determines that the critical entanglement spectrum is described by the CFT with a central charge $c \simeq 1$.

Moreover, the low-energy entanglement levels follow the finite-size scaling law under the three boundary conditions determined by the charge of the parent topological state m , which are displayed in Fig. 6(c) and (d). Since the large value of $L_A = 12$, there are finite-size corrections, which are order of $1/L_A^2$. In Fig. 7, we have carefully analyzed these corrections so that the entanglement levels are expressed in terms of the following primary fields: $(h, \bar{h}) = (0, 0), (3/4, 3/4), (0, 1/3)$, and $(3/4, 1/12)$ for the charge parent state with $m = 0$. On the other hand, for the parent topological state with $m = 1, 2$, the primary fields include $(1/3, 0), (1/12, 3/4), (1/12, 1/12)$ and $(1/3, 1/3)$. Note the momenta of some fields have been shifted by π in the presence the AFM correlation. Actually, all the primary fields can be further represented in terms of the primary fields of the compactified free boson CFT with the compactified radius $R = \sqrt{2/3}$,

$$h = \frac{1}{2} \left(\frac{\mathbf{e}}{R} + \frac{\mathbf{m}R}{2} \right)^2, \quad \bar{h} = \frac{1}{2} \left(\frac{\mathbf{e}}{R} - \frac{\mathbf{m}R}{2} \right)^2, \quad (38)$$

where \mathbf{e} denotes the electrical charge and \mathbf{m} is the magnetic winding number. In contrast to the critical statistical systems with both integers of \mathbf{e} and \mathbf{m} values, the quantum numbers (\mathbf{e}, \mathbf{m}) are found to be fractional and listed in Table. I.

So the quantum critical point separating a topological phase from its adjacent trivial phase is not necessarily unique, and we can in practice deduce a rich family of quantum critical theories to describe the phase transitions between them.

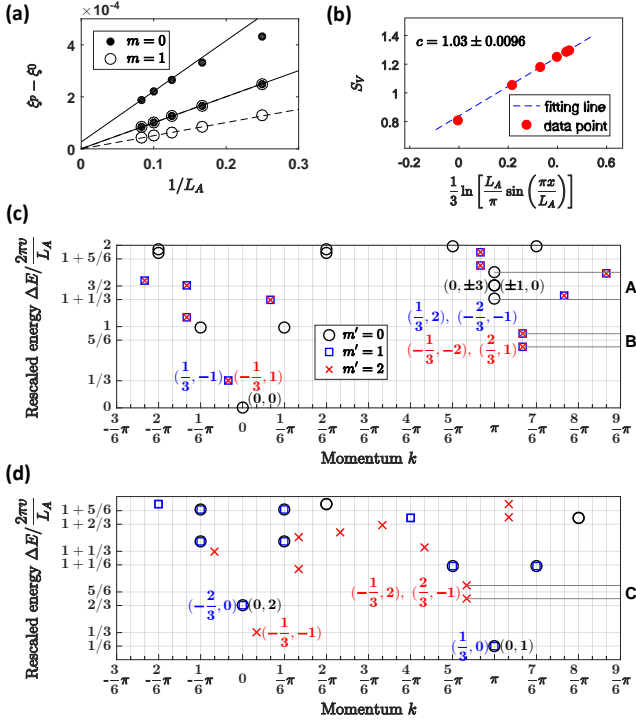


FIG. 6: (a) The finite-size scaling of the lowest two excited levels under the two different boundary conditions suggests a gapless entanglement spectrum in the thermodynamic limit. (b) The entanglement entropy of the ground state for the entanglement Hamiltonian S_V is calculated and the slope gives the central charge $c = 1.03 \pm 0.0096$. (c) The entanglement spectrum is obtained from the $m = 0$ parent topological state. (d) The entanglement spectrum is deduced from the $m = 1$ parent topological state. Some entanglement levels in (c) and (d) have strong finite-size corrections labeled by the letters A, B, C, whose errors are analysed in Fig.7. In both (c) and (d), m' denotes the total charge of the entanglement levels labeled by the quantum numbers (\mathbf{e}, \mathbf{m}) .

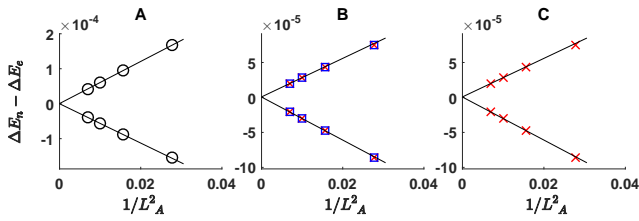


FIG. 7: The entanglement levels with large finite-size corrections marked by A, B, C in Fig. 6 (c) and (d) are numerically analysed, and those corrections are in order of $\mathcal{O}(1/L_A^2)$.

VI. DISCUSSION AND SUMMARY

To gain a better understanding of the numerical result, we could expand the logarithm of the reduced density operator Eq.(29) to obtain the leading terms of the bulk

TABLE I: The electric charge and winding quantum numbers and their degeneracies of the primary fields. m stands for the charge of the parent \mathbb{Z}_3 topological states, and m' denotes the total charge of the entanglement levels.

m	m'	(h, \bar{h})	(\mathbf{e}, \mathbf{m})	degeneracy
0	0	(0, 0)	(0, 0)	1
0	0	$(\frac{3}{4}, \frac{3}{4})$	$(\pm 1, 0), (0, \pm 3)$	4
0	1	$(0, \frac{1}{3})$	$(\frac{1}{3}, -1)$	1
0	1	$(\frac{3}{4}, \frac{1}{12})$	$(\frac{1}{3}, 2), (-\frac{2}{3}, -1)$	2
0	2	$(0, \frac{1}{3})$	$(-\frac{1}{3}, 1)$	1
0	2	$(\frac{3}{4}, \frac{1}{12})$	$(-\frac{1}{3}, -2), (\frac{2}{3}, 1)$	2
1	0	$(\frac{1}{12}, \frac{1}{12})$	(0, 1)	1
1	0	$(\frac{1}{3}, \frac{1}{3})$	(0, 2)	1
1	1	$(\frac{1}{12}, \frac{1}{12})$	$(\frac{1}{3}, 0)$	1
1	1	$(\frac{1}{3}, \frac{1}{3})$	$(-\frac{2}{3}, 0)$	1
1	2	$(\frac{1}{3}, 0)$	$(-\frac{1}{3}, -1)$	1
1	2	$(\frac{1}{12}, \frac{3}{4})$	$(-\frac{1}{3}, 2), (\frac{2}{3}, -1)$	2
2	0	$(\frac{1}{12}, \frac{1}{12})$	(0, -1)	1
2	0	$(\frac{1}{3}, \frac{1}{3})$	(0, -2)	1
2	1	$(\frac{1}{3}, 0)$	$(\frac{1}{3}, 1)$	1
2	1	$(\frac{1}{12}, \frac{3}{4})$	$(\frac{1}{3}, -2), (-\frac{2}{3}, 1)$	2
2	2	$(\frac{1}{12}, \frac{1}{12})$	$(-\frac{1}{3}, 0)$	1
2	2	$(\frac{1}{3}, \frac{1}{3})$	$(\frac{2}{3}, 0)$	1

entanglement Hamiltonian:

$$\hat{H}_A \simeq J_l \sum_{j=1}^{2L_A} \left[e^{i(\frac{\pi}{N} + l\theta_1)} \psi_j^\dagger \psi_{j+1} + h.c. \right] + L_A \ln N, \quad (39)$$

where the boundary condition is enforced by $\psi_{2L_A+1} \equiv e^{i\frac{2\pi}{N}(m-1)} \psi_1$. Since the couplings between the effective parafermions are mediated by the gapped bulk and decay exponentially with the correlation length $J_l = e^{-l/\xi}$, the subleading terms to be relatively negligible can be controlled by tuning $l/\xi \gg 1$. These leading Hamiltonian terms describe the nearest neighbor hopping of the edge parafermion modes and can indeed give rise to the quantum critical point between the topological phase and trivial phase¹⁴.

It should be noticed that the quantum critical point that we have extracted is more than just an isolated singular point, but indeed a phase transition point on a given path, which is hidden in the decoding operation. As we already mentioned, by tuning the relative block lengths l_A/l_B from larger than 1 to less than 1, the subsystem A can undergo a phase transition from the topological phase to the trivial phase with the same symmetry, by passing the topological quantum critical point.

In conclusion, we have generalized the recipe of de-

coding topological quantum criticality from topological wave-function to the strongly interacting long-range entangled topological phases. This is achieved by a non-trivial symmetric extensive interlaced bipartition and extraction of its entanglement spectrum. This is a novel recipe to extract topological quantum critical points from a gapped topological ground state, without any need for the parent Hamiltonian or choosing any specific perturbations. In general, using this method, we could obtain a family of critical points, for example the \mathbb{Z}_N ($N > 2$) parafermion phase. Moreover, we have provided more than just a method, but our method also has a rather strong implication of a general physical picture. Our result actually suggests an appealing generalization of the bulk-edge correspondence to bulk-edge-criticality correspondence. By some concrete exact demonstrations, we hope that our results in this paper combined with our earlier works on the bosonic symmetry-protected states should strongly support that the decoding recipe and the bulk-edge-criticality are universal in one-dimensional systems. This could potentially be further generalized to the intrinsic topological order in two-dimensional systems.

Acknowledgment.- The authors would like to thank Wen-Tao Xu and Hong-Hao Tu for their stimulating discussions and acknowledges the support of National Key Research and Development Program of China (2017YFA0302902).

Appendix A: Relationship between our parafermion MPS to the others

Our MPS is defined as the contraction of the local tensors in the graded space, whose graphic representation is shown in Fig. 8. It is a general \mathbb{Z}_N parafermionic MPS in the topological phase with the local matrix:

$$A_{\alpha,\beta}^{[k]} = C e^{-k\phi/N} \delta_{\beta-\alpha-k}. \quad (\text{A1})$$

For the \mathbb{Z}_2 case, there is an exact ground state with a fi-

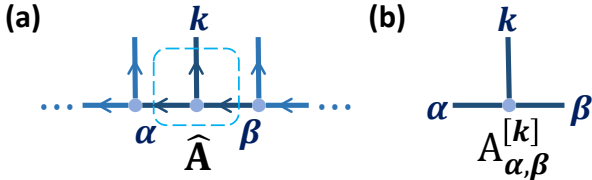


FIG. 8: (a) The graphical representation of the MPS built from the local tensor \hat{A} . An arrow pointing outwards from one site is associated to a super-vector space \mathbb{V}_F while inwards ones to \mathbb{V}_F^* . Contraction of the dual vector spaces tie neighboring sites together. (b) The graphical representation of the coefficient matrix $A^{[k]}$, where bonds imply the two virtual indices on both sides and one physical indices on the top.

nite correlation length found by H. Katsura, D. Schuricht,

and M. Takahashi¹²:

$$|\Psi_0\rangle = |\Psi^+\rangle + |\Psi^-\rangle, \quad |\Psi_1\rangle = |\Psi^+\rangle - |\Psi^-\rangle, \\ |\Psi^\pm\rangle = \frac{1}{(1+\alpha^2)^{L/2}} e^{\pm\alpha\hat{c}_1^\dagger} e^{\pm\alpha\hat{c}_2^\dagger} \dots e^{\pm\alpha\hat{c}_L^\dagger} |0\rangle, \quad (\text{A2})$$

where \hat{c}^\dagger is the fermionic creation operator, and α is a parameter related to the interaction strength. Because of the Pauli exclusion principle, all of the exponential terms can be expanded as $1 \pm \alpha\hat{c}_l^\dagger$, and all the higher order terms vanish completely, leading to a simple form of these two wave functions:

$$|\Psi_0\rangle \propto \sum_{\{k_l\}} |\alpha|^{\sum_{l=1}^L k_l} \delta_{(k_1+\dots+k_L) \bmod 2} |k_1 \dots k_L\rangle, \\ |\Psi_1\rangle \propto \sum_{\{k_l\}} |\alpha|^{\sum_{l=1}^L k_l} \delta_{(k_1+\dots+k_L-1) \bmod 2} |k_1 \dots k_L\rangle,$$

where the delta function restricts the parity of states to even or odd and the exponential part has been expressed as the local decaying factors. This can be further represented into the MPS form with the local tensor:

$$A_{\alpha,\beta}^{[k]} = e^{-k\phi/2} \delta_{(\beta-\alpha-k) \bmod 2}, \quad (\text{A3})$$

and $\phi = -2\ln|\alpha|$. Now it can be seen that this is nothing but the \mathbb{Z}_2 example of our general MPS.

Moreover, another exact solution of \mathbb{Z}_3 parafermionic ground state with a finite correlation length was proposed by F. Iemini, C. Mora, and L. Mazza¹³ in terms of the local tensor

$$A^{[k]} = \left(e^{-\phi/3} \sigma \right)^k, \quad \sigma = \begin{pmatrix} 1 & 0 & 0 \\ 0 & e^{i\frac{2\pi}{3}} & 0 \\ 0 & 0 & e^{i\frac{4\pi}{3}} \end{pmatrix}. \quad (\text{A4})$$

Via a gauge transformation U , we can transform this local tensor into another charge basis:

$$A'^{[k]} = U^\dagger A^{[k]} U = e^{-k\phi/3} \tau^k, \\ U = \frac{1}{\sqrt{3}} \begin{pmatrix} 1 & 1 & 1 \\ e^{i\frac{4\pi}{3}} & e^{i\frac{2\pi}{3}} & 1 \\ e^{i\frac{2\pi}{3}} & e^{i\frac{4\pi}{3}} & 1 \end{pmatrix}. \quad (\text{A5})$$

Then A' is exactly equal to the \mathbb{Z}_3 specific case of our general form. Although these two MPS are essentially equivalent to each other, our charge basis is a better choice. Under the open boundary condition, our MPS with dangling bond represents a topological state with zero parafermion modes, while their MPS with dangling bond does not have such clear physical meaning.

Appendix B: Transfer matrix and correlation functions

The transfer matrix defined in Eq.(12) can be expanded by the eigenvectors:

$$\mathbb{E}_{(\alpha,\alpha'),(\beta,\beta')} = \sum_{n,j} (R_{n,j})_{\alpha,\alpha'} \lambda_n (L_{n,j})_{\beta',\beta}. \quad (\text{B1})$$

It is very useful to calculate the two-point correlation function, which is generally defined by two local operators \hat{O}_1 and \hat{O}_2 with opposite charges. Assume that \hat{O}_1 is an operator with charge $-q$ on the lattice site l , while \hat{O}_2 is the other one with charge q on the lattice site $l+d$, which can be enforced on the local charge p state as:

$$\hat{O}_1|p\rangle \propto |(p-q) \bmod N\rangle, \hat{O}_2|p\rangle \propto |(p+q) \bmod N\rangle. \quad (\text{B2})$$

Putting them together ensures the zero total charge of the product operator. The correlation function is defined $\langle \Psi | \hat{O}_1 \hat{O}_2 | \Psi \rangle$ in a chain with L lattice sites, as shown in Fig. 9(a). No matter what the coefficient of the specific wave-function is, the contraction of the graded vector can be performed as:

$$\langle k'_L | \otimes_g \dots \otimes_g \langle k'_1 | \hat{O}_1 \hat{O}_2 | k_1 \rangle \otimes_g \dots \otimes_g | k_L \rangle. \quad (\text{B3})$$

Then the contractions can be divided into three parts. First, those bra parafermions in less than l site can be contracted after crossing two operators with zero total charge. The second is those bra parafermions from l to $l+d$ sites will be exchanged only with the operators \hat{O}_2 to be contracted, whose charge q leaves a phase factor $e^{-i\frac{2\pi}{N}q(k_l+\dots+k_{l+d})}$. And the remanent parafermions can be contracted normally without crossing any sites. It is almost similar to the correlation function for the bosonic case with an additional non-local phase between two operators. Fortunately, according to the bulk-edge correspondence, this phase factor can be represented in the virtual indices $e^{-i\frac{2\pi}{N}(\beta_{l+d-1}-\alpha_l)q}$, which gives rise to two gauge matrices behind the $d-2$ sites transfer matrix shown in Fig. 9(b).

Finally, the correlation function is written in a very simply form, where a unitary transform remains in the definition of the correlation length as shown:

$$\begin{aligned} \langle \hat{O}_1 \hat{O}_2 \rangle &= \frac{\langle \phi_L | \mathbb{E}^{l-1} \sigma^q \mathbb{E}_1 \mathbb{E}^{d-2} \sigma^{-q} \mathbb{E}_2 \mathbb{E}^{L-d-l} | \phi_R \rangle}{\langle \phi_L | \mathbb{E}^L | \phi_R \rangle} \\ &\simeq \left(\frac{\lambda_1}{\lambda_0} \right)^d \langle R_0 | \sigma^q \mathbb{E}_{O_1} | L_i \rangle \langle R_i | \sigma^{-q} \mathbb{E}_{O_2} | R_0 \rangle + h.c. \end{aligned} \quad (\text{B4})$$

where $\sigma_{\alpha,\beta} = e^{i\frac{2\pi}{N}\alpha} \delta_{\beta-\alpha}$ is the diagonal \mathbb{Z}_N charge matrix and $\mathcal{O}(|\lambda_2|^d)$ terms have been ignored. Then the correlation length can be straightforwardly derived and equal to that for two zero charged operators, as shown in Eq.(17).

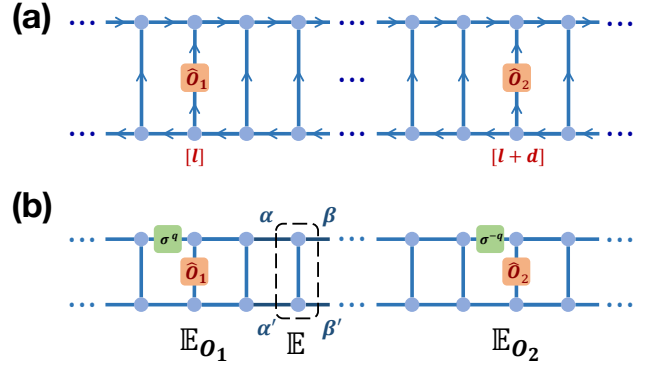


FIG. 9: (a) The definition of a correlation function between the operator O_1 with charge $-q$ on the lattice site l and the operator O_2 with charge q on the lattice site $l+d$ in the chain with length L . (b) The phase factor caused by those contraction can be expressed on the entangled basis.

Appendix C: Additional bonds in the parafermion MPO

The reduced density operator we are going to calculate is actually a parafermionic MPO, the contractions of which brings in nontrivial phase factors arising from the parafermion commutations. To deal with this, there is a trick to introduce additional bonds to keep track of the phase factor.

As shown in Fig. 3, the reduced density matrix can be obtained by contracting all of grouped physical indices in the subsystem B labeled by h, h' , leaving all of the grouped physical indices from the subsystem A labeled by p, q . This problem is not simple like the bosonic case, and all of contractions are carried out from the left as a convention. Now let's consider about an edge parafermion defined in the graded space of the j -th of the B part labeled by h_j , it will meet the corresponding partner labeled by h'_j only after crossing by the $j-1$ edge parafermions defined in the A part both on bra and ket chains, as shown in Fig. 10(a). Since the directions of exchanges in the bra and ket chains are opposite, they leave the phase factor conjugated to each other, which finally causes a phase factor $e^{i\frac{2\pi}{N}h_j \sum_{i<j} (p_i - q_i)}$. Those two parafermions labeled by h_j, h'_j form a bond state with zero charge, so no more phase factor is present in the next contraction. Here the local index h_j represents the virtual indices $\beta_j - \alpha_j - p_j$, therefore, two additional bonds in the j site are necessary to record the non-local total charges of parafermions crossed by the parafermions labeled by h_j , shown as in the r, l bonds of the tensor R (Eq.(27)). This is inspired from the previous work in the fermionic tensor contractions²¹. Finally, $r = l + (p - q)$ accumulates the charge and the phase factor is written into the local form as $e^{i\frac{2\pi}{N}l(\beta_j - \alpha_j - p_j)}$ for the j site.

Further more, the two virtual parafermions living on both of bra and ket chains constitute a single N -dimensional super-vector space, which can be represented

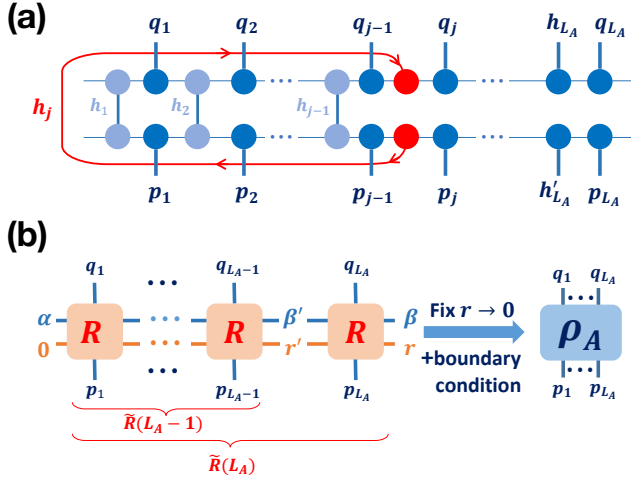


FIG. 10: (a) The parafermion defined on the j -th block of the part B can be contracted only after crossing $j-1$ parafermions in the part A on both the bra and ket chains. (b) The reduced density matrix can be obtained by considering the boundary conditions from the matrix product operator $\tilde{R}(L_A)$, whose unit cell is given by R . Those orange lines represent the additional bonds while the blue ones for the virtual and physical bonds.

as a single virtual bond. As the result, the reduced density matrix can be represented into a matrix product operator (MPO), as displayed in Fig. 10 with an omitted normalization factor $1/s_m(L)$ for the parent chain with charge m and length $L = 2lL_A$. The unit cell of the MPO is defined as R :

$$R_{(\alpha),(\beta r)}^{[p,q]} = \frac{1}{N^2} e^{i\frac{2\pi}{N}(\beta-\alpha-p)l} s_p s_q s_{\beta-\alpha-p}^2 \delta_{r-l-p+q}, \quad (\text{C1})$$

where the left-most bond l is fixed to zero as the start point and the final accumulated charge (the right-most r) is also fixed to zero.

To analyze the reduced density matrix for the subsystem A with L_A blocks, the matrix $\tilde{R}(L_A)$ can be solved mathematically, defined as Eq. (28) and shown in Fig. 10(b). After considering the boundary condition, the reduced density matrix can be expressed as

$$(\rho_A)_{\{q,p\}} = C' \left(\prod_{j=1}^{L_A} s_{p_j} \right) \tilde{I}_{\{P,Q\}} \left(\prod_{j=1}^{L_A} s_{q_j} \right). \quad (\text{C2})$$

where the singular values are diagonal contributions and \tilde{I} represents the non-diagonal contributions in the middle part of the reduced density matrix. In the charge accumulating basis, the reduced density matrix can be finally represented as:

$$\tilde{I}_{\{P,Q\}} = \delta_{P_{L_A}-Q_{L_A}} \sum_{k=0}^{N-1} \left[e^{i\frac{2\pi}{N}k(m-P_{L_A})} \lambda_k^l \prod_{j=1}^{L_A-1} \lambda_{k-P_j+Q_j}^l \right], \quad (\text{C3})$$

where $P_j = \sum_{i<j} p_i \pmod{N}$ and $Q_j = \sum_{i<j} q_i \pmod{N}$. Moreover, $C' = [N^{L_A} s_m^2 (2lL_A)]^{-1}$ in the expression of ρ_A is the common factor including the normalization factor for the finite length. From that form, it is easy verified the result given by Eq.(29), which is written in the basis of the edge parafermionic operators.

¹ G. Moore and N. Read, **360**, 362 (1991).

² H. Li and F. D. M. Haldane, Physical Review Letters **101**, 010504 (2008), URL <https://link.aps.org/doi/10.1103/PhysRevLett.101.010504>.

³ X.-L. Qi, H. Katsura, and A. W. W. Ludwig, Physical Review Letters **108**, 196402 (2012), URL <https://link.aps.org/doi/10.1103/PhysRevLett.108.196402>.

⁴ J. T. Chalker and P. D. Coddington, Journal of Physics C: Solid State Physics **21**, 2665 (1988), URL <http://stacks.iop.org/0022-3719/21/i=14/a=008>.

⁵ W.-J. Rao, X. Wan, and G.-M. Zhang, Phys. Rev. B **90**, 075151 (2014), URL <https://link.aps.org/doi/10.1103/PhysRevB.90.075151>.

⁶ Q. Zhu, X. Wan, and G.-M. Zhang, **90**, 235134 (2014), URL <https://link.aps.org/doi/10.1103/PhysRevB.90.235134>.

⁷ T. H. Hsieh and L. Fu, Phys. Rev. Lett. **113**, 106801 (2014), URL <https://link.aps.org/doi/10.1103/PhysRevLett.113.106801>.

⁸ L. Fidkowski and A. Kitaev, Phys. Rev. B **81**, 134509 (2010), URL <https://link.aps.org/doi/10.1103/PhysRevB.81.134509>.

⁹ N. Bultinck, D. J. Williamson, J. Haegeman, and F. Verstraete, Phys. Rev. B **95**, 075108 (2017), URL <https://link.aps.org/doi/10.1103/PhysRevB.95.075108>.

¹⁰ W.-T. Xu and G.-M. Zhang, Phys. Rev. B **95**, 195122 (2017), URL <https://link.aps.org/doi/10.1103/PhysRevB.95.195122>.

¹¹ W.-T. Xu and G.-M. Zhang, Phys. Rev. B **97**, 035160 (2018), URL <https://link.aps.org/doi/10.1103/PhysRevB.97.035160>.

¹² H. Katsura, D. Schuricht, and M. Takahashi, Phys. Rev. B **92**, 115137 (2015), URL <https://link.aps.org/doi/10.1103/PhysRevB.92.115137>.

¹³ F. Iemini, C. Mora, and L. Mazza, Phys. Rev. Lett. **118**, 170402 (2017), URL <https://link.aps.org/doi/10.1103/PhysRevLett.118.170402>.

¹⁴ W. Li, S. Yang, H.-H. Tu, and M. Cheng, Phys. Rev. B **91**, 115133 (2015), URL <https://link.aps.org/doi/10.1103/PhysRevB.91.115133>.

¹⁵ Y. Zhuang, H. J. Changlani, N. M. Tubman, and T. L. Hughes, Physical Review B **92**, 035154 (2015), URL <https://link.aps.org/doi/10.1103/PhysRevB.92.035154>.

- ¹⁶ D. F. Mross, J. Alicea, and O. I. Motrunich, *Phys. Rev. X* **7**, 041016 (2017), URL <https://link.aps.org/doi/10.1103/PhysRevX.7.041016>.
- ¹⁷ T. H. Hsieh, G. B. Halász, and T. Grover, *Phys. Rev. Lett.* **117**, 166802 (2016), URL <https://link.aps.org/doi/10.1103/PhysRevLett.117.166802>.
- ¹⁸ P. Calabrese and J. Cardy, *Journal of Physics A: Mathematical and Theoretical* **42**, 504005 (2009), URL <http://stacks.iop.org/1751-8121/42/i=50/a=504005>.
- ¹⁹ M. Greiter, V. Schnells, and R. Thomale, *Annals of Physics* **351**, 1026 (2014), ISSN 0003-4916, URL <http://www.sciencedirect.com/science/article/pii/S0003491614002498>.
- ²⁰ B. K. Chakrabarti and A. Das, in *Quantum Annealing and Other Optimization Methods* (Springer, Berlin, Heidelberg, 1996), *Lecture Notes in Physics*, pp. 1–36, ISBN 978-3-540-27987-7 978-3-540-31515-5, doi: 10.1007/11526216_1, URL https://link.springer.com/chapter/10.1007/11526216_1.
- ²¹ C. V. Kraus, N. Schuch, F. Verstraete, and J. I. Cirac, *Phys. Rev. A* **81**, 052338 (2010), URL <https://link.aps.org/doi/10.1103/PhysRevA.81.052338>.